Fluorescence molecular imaging for identification of high-grade dysplasia in patients with head and neck cancer

Fakurnejad, S.; van Keulen, S.; Nishio, N.; Engelen, M.; van den Berg, N.S.; Lu, G.; Birkeland, A.; Baik, F.; Colevas, A.D.; Rosenthal, E.L.; Martin, B.A.

DOI
10.1016/j.oraloncology.2019.08.008

Publication date
2019

Document Version
Final published version

Published in
Oral Oncology

Oral Oncology 97 (2019) 50–55

Contents lists available at ScienceDirect

Oral Oncology

journal homepage: www.elsevier.com/locate/oraloncology

Fluorescence molecular imaging for identification of high-grade dysplasia in patients with head and neck cancer

Shayan Fakurnejad[a], Stan van Keulen[a,b], Naoki Nishio[a], Myrthe Engelen[a], Nynke S. van den Berg[a], Guolan Lu[a], Andrew Birkeland[a], Fred Baik[a], A. Dimitrios Colevas[c], Eben L. Rosenthal[a], Brock A. Martin[d,*]

[a] Department of Otolaryngology, Stanford University School of Medicine, 900 Blake Wilbur Drive, Stanford, CA 94305, United States
[b] Department of Oral and Maxillofacial Surgery, Amsterdam University Medical Center, De Boelelaan 1118, 1081 HV Amsterdam, the Netherlands
[c] Department of Medicine, Division of Medical Oncology, University School of Medicine, 269 Campus Drive, Stanford, CA 94305, United States
[d] Department of Pathology, Stanford University School of Medicine, 291 Campus Drive, Stanford, CA 94305, United States

ARTICLE INFO

Keywords:
Near-infrared
Fluorescence imaging
Molecular imaging
Dysplasia
Head and neck cancer
Oral cavity
Antibody

ABSTRACT

Objective: High-grade dysplasia is associated with a risk of malignant transformation, and it is necessary to distinguish from normal epithelium or low-grade dysplasia, especially in the intraoperative setting. We hypothesize that an anti-epidermal growth factor receptor (EGFR) contrast agent can be used to differentiate high-grade dysplasia from low-grade dysplasia and normal epithelium.

Materials and methods: Patients with biopsy proven head and neck squamous cell carcinoma (HNSCC) were enrolled in a clinical trial using systemically injected fluorescently labeled anti-EGFR antibody (panitumumab-IRDye800CW) (NCT02415881). Paraffin embedded tumor specimens from 11 patients were evaluated by fluorescence histopathology. Hematoxylin and eosin (H&E) slides were reviewed by a board-certified pathologist, and regions of invasive squamous cell carcinoma, high-grade dysplasia and low-grade dysplasia were delineated. EGFR expression was assessed for each patient by way of immunohistochemistry.

Results: 11 patients were included in the study with a total of 219 areas on tissue sections analyzed; 68 normal epithelium, 53 low-grade dysplasia, 48 high-grade dysplasia, and 50 malignant regions. The signal-to-background ratio (SBR) increased proportionally with increasing grade of dysplasia; normal epithelium (1.5 ± 0.1), low-grade dysplasia (1.8 ± 0.1), high-grade dysplasia: (2.3 ± 0.2). High-grade dysplasia had a significantly higher SBR when compared to normal or low-grade dysplasia ($p < 0.05$). Fluorescence histopathology positively correlated with EGFR expression by immunohistochemistry, which also increased proportionally with increasing degree of dysplasia.

Conclusion: Molecular imaging with an anti-EGFR agent can successfully discriminate high-grade dysplastic lesions from low-grade dysplasia and normal epithelium.

Introduction

Field cancerization and mucosal dysplasia pose a significant diagnostic challenge with serious implications for patient outcomes [1,2]. As a result, there is significant interest in the development of real-time, widefield imaging strategies for the detection of pre-malignant and early stage malignant lesions. Recent studies suggest that malignant transformation is found in 12.1% (range 0–36.4%) of patients with any degree of dysplasia, with a median follow-up of 1.5–10 years [3]. However, patients with high-grade dysplasia (HGD) have a 2-fold higher chance of malignant transformation when compared to low-grade dysplasia (LGD), at around 24.1% (range 13.3–39.5%) [3]. Furthermore, the presence of low-grade, including mild to moderate, dysplasia at the surgical margins is associated with increased local recurrence rates and poorer patient outcomes, and as such, detection of pre-malignant disease is of importance in the operating room as well [1,2]. Unfortunately, these lesions are very difficult to detect and diagnose without histopathologic assessment. Although topical

* Corresponding author at: Department of Pathology, 300 Pasteur Drive, Lane 235, Stanford, CA 94305, United States.
E-mail addresses: shayanf@stanford.edu (S. Fakurnejad), stanvk@stanford.edu (S. van Keulen), nn240@stanford.edu (N. Nishio), mengelen@stanford.edu (M. Engelen), nsvdb@stanford.edu (N.S. van den Berg), guolanlu@stanford.edu (G. Lu), abirkela@stanford.edu (A. Birkeland), fbaik@stanford.edu (F. Baik), colevas@stanford.edu (A.D. Colevas), elr@stanford.edu (E.L. Rosenthal), brockm@stanford.edu (B.A. Martin).

https://doi.org/10.1016/j.oraloncology.2019.08.008
Received 11 March 2019; Received in revised form 15 July 2019; Accepted 6 August 2019
Available online 12 August 2019

Table 1
Summary of patient characteristics. Smoking and alcohol use includes whether patients were currently using, or if there was a history of use.

Patient	Age	Gender	Tumor location	Smoking status	Alcohol use
1	56	M	Buccal	27 pack-year history	None
2	52	M	Floor of mouth	10 pack-years	3–4 drinks/week
3	69	F	Buccal	None	None
4	85	M	Larynx	40 pack-year history	4–5 drinks/week
5	54	M	Buccal	45 pack-years	None
6	71	M	Tongue	30 pack-year history	None
7	65	F	Buccal	45 pack-year history	1–2 drinks/week
8	63	F	Alveolar ridge	None	Rare
9	71	F	Tongue	None	None
10	71	F	Floor of mouth	None	None
11	59	F	Tongue	8.5 pack-years	History of alcohol abuse

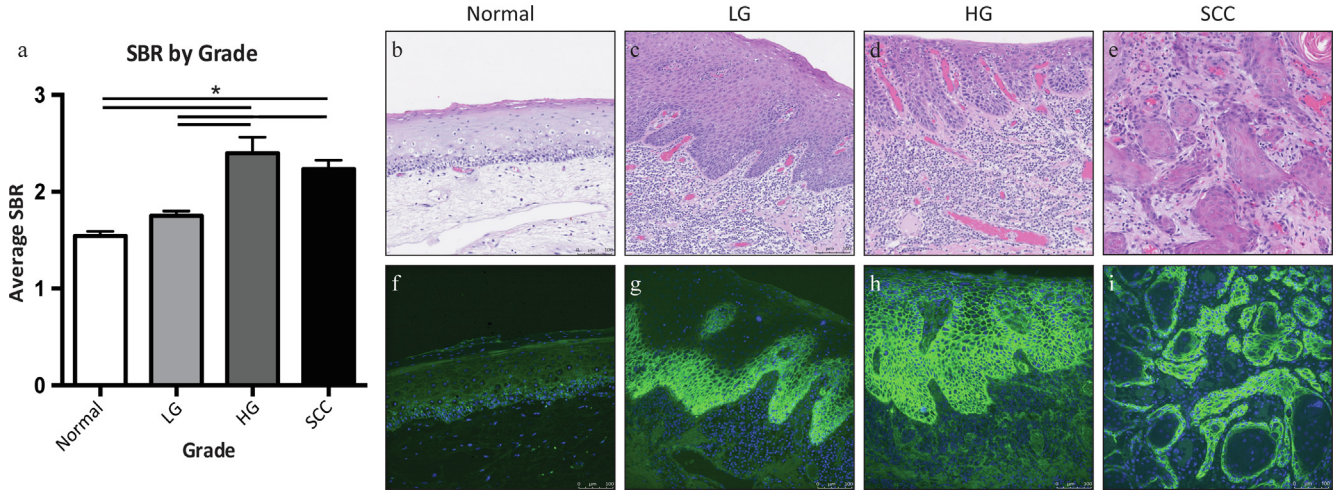

Fig. 1. Fluorescence histopathology of 10 μm slides from patient specimen. (a) Average SBR, with standard error of the mean, for each grade. (b-i) Representative images of the H&E (top) and fluorescence (bottom) for each of the grades. Representative images of (b,f) normal epithelium, (c,g) low-grade dysplasia, (d,h) high-grade dysplasia, and (e,i) invasive squamous cell carcinoma. LG = low-grade dysplasia, HG = high-grade dysplasia, SCC = squamous cell carcinoma. Statistical analysis by Mann-Whitney *U* test.

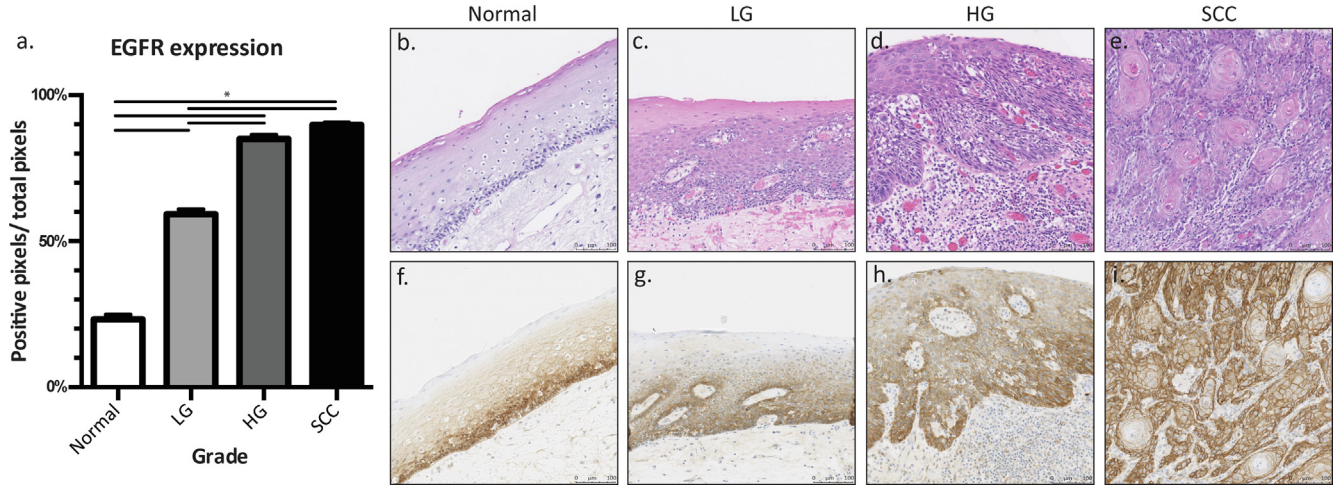

Fig. 2. EGFR immunohistochemistry staining of 10 μm slides from patients specimen. (a) EGFR expression, with standard error, of the 10 μm slides by grade. (b-i) Representative images of the H&E (top) and IHC (bottom) for each of the grades. Representative images for (b,f) normal epithelium, (c,g) low-grade dysplasia, (d,h) high-grade dysplasia, and (e,i) invasive squamous cell carcinoma. LG = low-grade dysplasia, HG = high-grade dysplasia, SCC = squamous cell carcinoma. Statistical analysis by Mann-Whitney *U* test.

application and imaging technologies, including high resolution magnifying endoscopy (HRME) and optical coherence tomography (OCT), have been developed for *in vivo* histological evaluation of tissues, these methods are not able to evaluate the surgical view [4–7]. This ultimately results in similar challenges as with tissue biopsy, namely sampling error, time, and cost [8]. An ideal system would be highly specific, allow for rapid assessment of the entire field, and involve minimal burden on the patient.

Activation and upregulation of EGFR is a known phenomenon in HNSCC, with up to 90% of all HNSCC overexpressing EGFR [9,10].

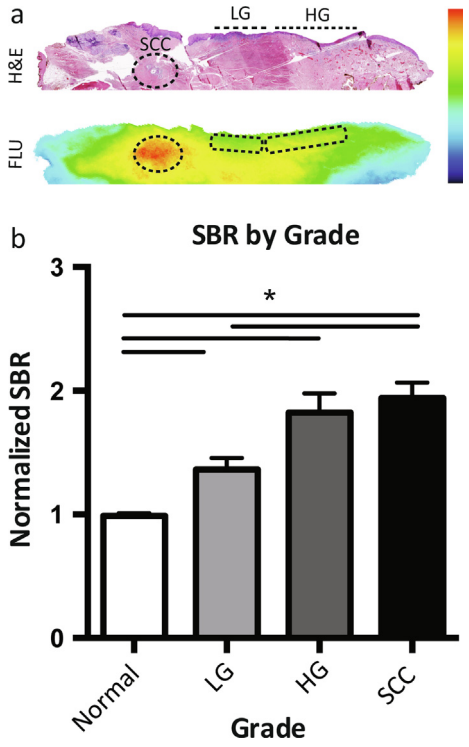

Fig. 3. Fluorescence imaging of macroscopic sections from patient specimen. (a) One representative H&E with regions of interest outlined (top) and the corresponding fluorescence image of the macroscopic tissue section with the corresponding regions delineated (bottom). (b) Average SBR (with standard error bars) of the 5 mm, macroscopic tissue sections by grade. LG = low-grade dysplasia, HG = high-grade dysplasia, SCC = squamous cell carcinoma. Statistical analysis by Mann-Whitney *U* test.

Conveniently, this transmembrane receptor is also upregulated in countless other solid tumors, and as such, this target has become a mainstay in oncologic therapies [11,12]. Recently, this has been leveraged for detection and diagnosis of cancers by functionalizing humanized anti-EGFR antibodies with fluorescent tracers with promising results [13–15]. This has been particularly effective for fluorescence-guided surgery. Moreover, it is also known that dysplastic epithelium overexpresses EGFR, with expression increasing linearly with increasing degree of dysplasia [16]. Given this important point, we hypothesized that an anti-EGFR antibody could be an effective means to delineate dysplasia.

The primary aim of this study was to demonstrate differences in EGFR expression between dysplastic epithelium and normal epithelium, and secondly to leverage this in order to detect areas of dysplasia in surgical specimens obtained from patients with HNSCC; if successful, this technique could be used to identify areas of high-grade dysplasia and facilitate complete resections intraoperatively, as well as set the groundwork for a potential screening tool of pre-malignant lesions in the clinic.

Methods

Study design

The phase I study protocol was approved by the Stanford University Institutional Review Board (IRB-35064) and the FDA (NCT02415881), and written informed consent was obtained from all patients. The study was performed in accordance with the Helsinki Declaration of 1975 and its amendments, FDA's ICH-GCP guidelines, and the laws and regulations of the United States.

All patients with biopsy-proven, primary or recurrent HNSCC scheduled to undergo standard of care surgery with curative intent were eligible. Patients received an infusion of panitumumab-IRDye800CW, intravenously 1–5 days prior to surgery, and fluorescence imaging was obtained before, during, and after surgery as previously described [13,17].

Patients were then retrospectively included in this study on the basis of dysplasia being noted by the pathologist on the initial hematoxylin and eosin (H&E) sections generated as part of standard of care. Tissue sections were pulled and re-assessed by the pathologist to further delineate regions of dysplasia and invasive carcinoma.

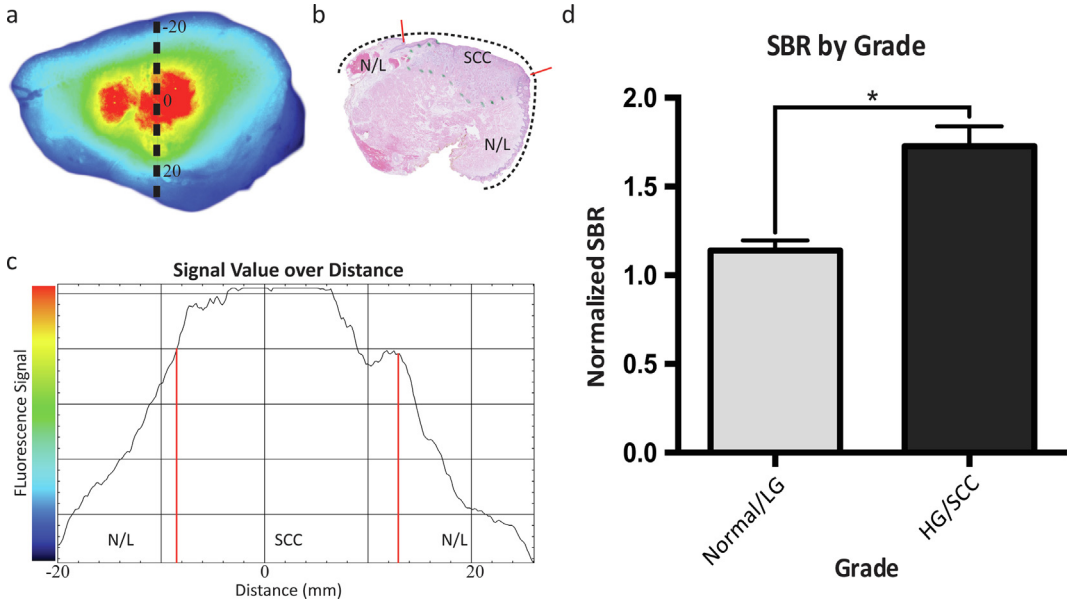

Fig. 4. Fluorescence imaging of whole patient specimen. (a) A representative fluorescence image of a specimen. The dotted line corresponds to (b) the H&E with regions of interest delineated. (d) The signal value curve over the representative line displayed in (a-b). (c) Average SBR, with standard error, of the whole specimen for Normal/LG and HG/SCC tissue. LG = low-grade dysplasia, HG = high-grade dysplasia, SCC = squamous cell carcinoma, N/L = normal-to-low grade. Statistical analysis by Mann-Whitney *U* test.

Tissue processing

Intraoperatively, tumors were resected per standard of care, with fluorescence-guidance augmenting surgical decision-making [13,17]. After resection, specimens were formalin-fixed overnight and serially sectioned into 5 mm-thick macroscopic cross-sections, referred to as macrosections, which were occasionally additionally bi- or trisected to fit into cassettes for processing as formalin-fixed and paraffin-embedded (FFPE) tissue blocks. Microscopic sections (5 μm in thickness) were then cut from each tissue block, and standard histopathological assessment of routine H&E-stained slides was conducted by a board-certified pathologist with expertise in head and neck pathology. To assess the varying grades of dysplasia, the pathologist outlined regions of low-grade dysplasia (LGD), high-grade dysplasia (HGD), and invasive squamous cell carcinoma (SCC) on the H&E slides, as well as regions of non-dysplastic epithelium for reference. A two-tiered grading system was utilized to simplify the analysis and increase statistical power of this small study while maintaining clinically meaningful groups. The pathologist was blinded from the fluorescence images for the entirety of the study.

Fluorescence imaging acquisition and analysis

Fluorescence images were taken before, during, and after surgical resection as previously described [13,17]. Directly after tumor resection, whole specimens were imaged *ex vivo* in a closed-field specimen imager (IGP-Elvis, LI-COR Biosciences, Lincoln, NE USA) [18]. Subsequently FFPE blocks were imaged using the Odyssey CLx imaging platform (LI-COR Biosciences, Lincoln, NE USA). From each FFPE block, slides were cut for H&E staining as well as two blank slides (5 μm) for fluorescence imaging and immunohistochemical staining, respectively. The 5 μm blank slides were then imaged using the Odyssey CLx imaging platform (LI-COR Biosciences, Lincoln, NE, USA) to identify fluorescence signal within the regions of interest (ROI) corresponding to the H&E delineations from the pathologist. Subsequently, the H&E slides were mapped back to the original tissue blocks (n = 5 patients) and eventually to the complete primary tumor (n = 3 patients).

To estimate signal-to-background ratios (SBRs), ROIs were drawn around areas of malignant, dysplastic, or normal epithelium, as outlined by the pathologist. Subsequently, the SBR was calculated by dividing the mean fluorescence intensity (MFI) of the ROI (i.e. malignant, dysplastic, or normal epithelium) by the MFI of the background signal (i.e. adjacent uninvolved tissue, generally skeletal muscle). For the tissue blocks, the same analysis was performed to calculate SBR; however, the SBR of each region was then normalized to normal epithelium, as delineated by the pathologist, to account for differences in total fluorescence between the blocks.

For whole specimen analysis, each specimen was virtually reconstructed from the macroscopic tissue sections, allowing for histologic mapping of the microscopic tissue sections. After cross-sectioning, a brightfield image was taken of the sectioned specimen and annotated to ensure accurate registration of each macrosection to its original location. Each macrosection was placed into corresponding tissue block (s), as annotated in the brightfield image. The slides cut from each tissue block were then registered to the original location within the primary specimen, allowing accurate reconstruction. To further ensure accurate reconstructions, only patients with multiple contiguous slides containing dysplasia were included in the whole specimen analysis. ImageJ (U.S. NIH, Bethesda, MD USA) was used to measure fluorescence intensity using a line analysis along the segment corresponding to the tissue section. Regions from the fluorescence intensity curve were correlated to the various grades on the outlined H&E slides; from here, SBRs were calculated in similar fashion as described above with the background being set as adjacent normal epithelium as underlying muscle was not always visible. All averages were provided with standard error of the mean.

Data was loaded into Prism 6.0 (GraphPad Software, San Diego, CA USA), and groups were compared using a Mann–Whitney *U* test. A p-value of 0.05 or less was considered statistically significant.

EGFR immunohistochemistry and quantification

To ensure that EGFR expression did indeed vary between the grades of dysplasia and was the primary basis for the localization of the antibody-dye complex, conventional immunohistochemistry for EGFR was also applied. Antigen retrieval was performed, and slides were stained using a slide autostainer in standard fashion (Dako Link 48 and PT Link, Agilent Technologies Inc., Santa Clara, CA, USA). Briefly, the slides were blocked with EnVision FLEX Peroxidase-Blocking reagent (Dako SM801), incubated for 20 min in EGFR primary antibody (ThermoScientific, Clone EP38Y), and visualized using the Dako FLEX + Rabbit visualization system (Dako SM802, SM803, SM805). Counterstain was performed with hematoxylin (Dako SM806). Slides were then coverslipped and digitized at 200x magnification using a high-resolution slide scanner (NanoZoomer 2.0-RS, Hamamatsu Photonics, Hamamatsu City, Japan).

Digitized slides were then loaded into Aperio ImageScope (Leica Biosystems Imaging Inc., Vista, CA USA). In ImageScope, 5 representative areas were randomly picked for each ROI of normal epithelium, LGD, HGD, and SCC. A hue value of 0.1 was chosen in ImageScope to detect the brown colored pixels that indicate EGFR expression. For each area, the number of pixels with a value below 0.1 was calculated using the Aperio Positive Pixel Count Algorithm (Leica Biosystems Imaging Inc., Vista, CA USA). This algorithm assigns each pixel as strongly positive, positive, or weakly positive. Weakly positive was considered equivalent to the background signal. For each area, the total number of strongly positive and positive pixels is divided by the total number of pixels in that area. Averages were calculated for each ROI based on the 5 representative areas, and a similar comparison between groups was performed as described above.

Results

Microscopic data

Eleven patients were enrolled in this study, and the patient characteristics are summarized in Table 1. After H&E evaluation of all tissue sections, a total of 44 FFPE blocks were selected based on the presence of normal epithelium, LGD, HGD, and SCC, and were further sectioned to characterize EGFR expression and subsequent fluorescence histopathology. From these blocks 219 ROIs were selected; 68 regions of normal epithelium, 53 regions of LGD, 48 regions of HGD, and 50 regions of SCC. Nine out of eleven patients (81.8%) had HGD present on at least one slide. The average mean fluorescence intensity (MFI) was 1.5 ± 0.1, 2.0 ± 0.1, 3.2 ± 0.4, and 2.3 ± 0.1 for normal, LGD, HGD, and SCC, respectively. When evaluating the signal compared to background fluorescence (the fluorescent signal of adjacent muscle), the average signal to noise ratio (SBR) was 1.5 ± 0.1, 1.8 ± 0.1, 2.3 ± 0.2, and 2.2 ± 0.1 for the same histologic grades, respectively (Fig. 1). HGD and SCC regions had significantly higher SBRs when compared to LGD and normal ($p < 0.05$). By immunohistochemistry, EGFR expression was found to increase with advancing grades of dysplasia, with the strongest expression found in regions of SCC (Fig. 2). The grade of dysplasia correlated with the percent area of EGFR expression; 23.2 ± 0.2%, 59.3 ± 0.2%, 85.0 ± 0.3%, and 89.8 ± 0.1% for normal, LGD, HGD, and SCC respectively. HGD and SCC had significantly elevated EGFR expression compared to LGD and normal ($p < 0.05$), and LGD had significantly stronger EGFR staining than normal ($p < 0.05$).

Evaluation of tissue blocks

Five patients were found to have all four grades of epithelium (normal, LGD, HGD, and SCC) represented in the same tissue specimen allowing for direct comparison of imaging results. From these five patients, 21 tissue blocks were analyzed, yielding 86 ROIs; 24 regions of normal epithelium, 20 regions of LGD, 17 regions of HGD, and 25 regions of SCC. SBR was calculated by comparing normal epithelium (background) to LGD (1.4 ± 0.02), HGD (1.8 ± 0.5), and SCC (1.9 ± 0.02) (Fig. 3). A statistically significant difference was found between SCC and LGD, as well as between HGD and LGD ($p < 0.05$), but not between HGD and SCC. All premalignant and malignant tissues had a statistically significantly higher average SBR when compared to normal ($p < 0.05$).

Evaluation of whole tissue

Four primary tumor specimens were included in the analysis. One patient, for which multiple contiguous slides were available, was excluded due to an inability to accurately reconstruct the primary specimen. For the remaining three patients, it was possible to virtually reconstruct the primary specimen from the individual brightfield images of macrosections, allowing the registration of H&E histology to the original location within the specimen. Due to the small sample size and the fact that normal and LGD can be monitored whereas HGD and SCC would be acted upon in a similar fashion clinically, normal and LGD were grouped, and HGD and SCC were grouped. There was a total of 26 normal-to-LGD and 19 HGD-to-SCC regions analyzed by fluorescence imaging of the *ex vivo* whole tissue specimen. The average SBR for normal-to-LGD and HGD-to-SCC was 1.14 ± 0.11 and 1.73 ± 0.03, respectively, which was statistically significantly different ($p < 0.05$)(see Fig. 4).

Discussion

In this study, we reviewed primary tumor specimens from HNSCC patients undergoing intraoperative molecular imaging to evaluate whether an anti-EGFR molecular imaging agent can accurately distinguish escalating grades of dysplasia from normal epithelium. Interestingly, we found that 81.8% of patients in the study had high-grade dysplasia present on at least one tissue section. However, dysplasia can be significantly more challenging to detect, both preoperatively and intraoperatively for surgeons as well as for surgical pathologists, when compared to invasive carcinoma, despite having serious patient implications, such as increased locoregional recurrence rates, if left untreated [1,2]. Fluorescence histopathology demonstrated that fluorescence positively correlates with grade of dysplasia on a microscopic level, with HGD having greater uptake of the optical contrast agent, and thus greater levels of fluorescence signal, compared to LGD and normal epithelium. In fact, the fluorescent signal of HGD in this study was similar to SCC. Evaluation of the tissue sections on a macroscopic level and subsequently on the primary specimen, showed that these results held true. Furthermore, we demonstrated that increasing grades of dysplasia correlated with EGFR expression based on digital quantification of EGFR immunohistochemical staining.

It remains challenging to distinguish dysplasia from normal epithelium intraoperatively and numerous techniques have been evaluated to improve its detection. For example, topical agents such as acetic acid and toluidine blue have been used for decades, and although these have relatively low cost and patient burden, they lack sufficient specificity and sensitivity for detecting dysplasia [8]. Other imaging technologies such as OCT and HRME have been tested repeatedly, and some are available for commercial use, but these have not been adopted in the management of HNSCC because of the challenges with use in the oral cavity and the very limited field of view (often less than 1–2 mm) [5,22]. Autofluorescence imaging and *in vivo* microscopy techniques have significant potential but require specific knowledge of histological diagnosis (or partnership with pathology) and much like ultrasound, can be difficult to acquire the data and document the results [8]. Our findings demonstrate that SCC and HGD can be selectively identified from adjacent LGD and normal epithelium by molecular imaging. Although we found no statistical difference between SCC and HGD, both lesions were easily differentiated compared to adjacent normal epithelium. While only a small subset of cases in the current study were available for analysis at the whole specimen level, and grouping the lesions into those that require clinical action and those that do not was necessary, our data suggest that anti-EGFR based intraoperative molecular imaging technology may be able to delineate normal and LGD from HGD and malignant lesions. If successfully implemented, the use of widefield real-time imaging might improve tumor resection and significantly decrease time and financial cost while improving patient outcomes [8].

Our analysis was limited to patients undergoing excision of an invasive carcinoma and conducted on dysplasia arising in adjacent mucosa. While it is important to intraoperatively detect surgically actionable HGD, analysis of patients with HGD and no invasive carcinoma may not provide the same result, and such a study is warranted to more accurately determine the efficacy of EGFR-based molecular imaging for early detection of HGD. An inherent limitation of studying grades of dysplasia is the poor interobserver reproducibility for histopathologic diagnosis, particularly with respect to LGD, which is challenging to distinguish from reactive or hyperplastic epithelium [23].

Nevertheless, in this study we have shown that anti-EGFR molecular imaging using panitumumab-IRDye800CW has potential for detection of premalignant lesions that may go unnoticed or require frozen section for confirmation intraoperatively. We have provided data that demonstrates that EGFR expression varies between dysplastic epithelium and normal epithelium, positively correlating with increasing degrees of dysplasia, and that a fluorescence molecular imaging agent positively correlates with worsening dysplasia on the microscopic and macroscopic scale. Furthermore, we contend this study provides the necessary foundation for testing an anti-EGFR molecular imaging as a potential screening tool for early detection of high-grade dysplasia in the clinic.

Conclusion

Anti-EGFR molecular imaging has the potential to successfully discriminate LGD and HGD lesions from SCC and normal epithelium on fluorescence histopathology. We posit that our data can encourage future studies assessing fluorescence imaging for intraoperative detection of dysplasia, and as a potential screening tool for detection of premalignant lesions in clinic.

Declaration of Competing Interest

None declared.

Acknowledgements

This work was supported in part by the Stanford Comprehensive Cancer Center, the Stanford University School of Medicine Medical Scholars Program, the Netherlands Organization for Scientific Research (Rubicon; 019.171LW.022), the National Institutes of Health and the National Cancer Institute (R01CA190306), the Stanford Molecular Imaging Scholars (SMIS) program (T32CA118681) and institutional equipment loans from Novadaq and LI-COR Biosciences Inc.

References

[1] Gokavarapu S, Parvataneni N, Pavagada S, Chandrasekhara Rao LM, Raju KV, Rao TS. Mild to moderate dysplasia at surgical margin is a significant indicator of survival in patients with oral cancer. Oral Surg Oral Med Oral Pathol Oral Radiol

2017;123(3):330–7.
[2] Weijers M, Snow GB, Bezemer PD, van der Wal JE, van der Waal I. The clinical relevance of epithelial dysplasia in the surgical margins of tongue and floor of mouth squamous cell carcinoma: an analysis of 37 patients. J Oral Pathol Med 2002;31(1):11–5.
[3] Mehanna HM, Rattay T, Smith J, McConkey CC. Treatment and follow-up of oral dysplasia - a systematic review and meta-analysis. Head Neck 2009;31(12):1600–9.
[4] Patsias A, Giraldez-Rodriguez L, Polydorides AD, et al. Feasibility of transoral robotic-assisted high-resolution microendoscopic imaging of oropharyngeal squamous cell carcinoma. Head Neck 2015;37(8):E99–102.
[5] Muldoon TJ, Roblyer D, Williams MD, Stepanek VM, Richards-Kortum R, Gillenwater AM. Noninvasive imaging of oral neoplasia with a high-resolution fiber-optic microendoscope. Head Neck 2012;34(3):305–12.
[6] Yang EC, Schwarz RA, Lang AK, et al. In vivo multimodal optical imaging: improved detection of oral dysplasia in low-risk oral mucosal lesions. Cancer Prev Res (Phila) 2018;11(8):465–76.
[7] Ridgway JM, Armstrong WB, Guo S, et al. In vivo optical coherence tomography of the human oral cavity and oropharynx. Arch Otolaryngol Head Neck Surg 2006;132(10):1074–81.
[8] Yang EC, Tan MT, Schwarz RA, Richards-Kortum RR, Gillenwater AM, Vigneswaran N. Noninvasive diagnostic adjuncts for the evaluation of potentially premalignant oral epithelial lesions: current limitations and future directions. Oral Surg Oral Med Oral Pathol Oral Radiol 2018;125(6):670–81.
[9] Rubin Grandis J, Melhem MF, Gooding WE, et al. Levels of TGF-alpha and EGFR protein in head and neck squamous cell carcinoma and patient survival. J Natl Cancer Inst 1998;90(11):824–32.
[10] Grandis JR, Tweardy DJ. Elevated levels of transforming growth factor alpha and epidermal growth factor receptor messenger RNA are early markers of carcinogenesis in head and neck cancer. Cancer Res 1993;53(15):3579–84.
[11] Ciardiello F, Tortora G. EGFR antagonists in cancer treatment. N Engl J Med 2008;358(11):1160–74.
[12] Vokes EE, Chu E. Anti-EGFR therapies: clinical experience in colorectal, lung, and head and neck cancers. Oncology (Williston Park) 2006;20(5 Suppl 2):15–25.
[13] Gao RW, Teraphongphom NT, van den Berg NS, et al. Determination of tumor margins with surgical specimen mapping using near-infrared fluorescence. Cancer Res 2018;78(17):5144–54.
[14] Rosenthal EL, Warram JM, de Boer E, et al. Safety and tumor specificity of cetuximab-IRDye800 for surgical navigation in head and neck cancer. Clin Cancer Res: Official J Am Assoc Cancer Res 2015;21(16):3658–66.
[15] Samkoe KS, Gunn JR, Marra K, et al. Toxicity and pharmacokinetic profile for single-dose injection of ABY-029: a fluorescent anti-EGFR synthetic affibody molecule for human use. Mol Imaging Biology: MIB: Official Publ Acad Mol Imaging 2017;19(4):512–21.
[16] Shin DM, Ro JY, Hong WK, Hittelman WN. Dysregulation of epidermal growth factor receptor expression in premalignant lesions during head and neck tumorigenesis. Cancer Res 1994;54(12):3153–9.
[17] van Keulen S, Nishio N, Fakurnejad S, et al. The clinical application of fluorescence-guided surgery in head and neck cancer. J Nucl Med: Official Publ, Soc Nucl Med 2019.
[18] van Keulen S, van den Berg NS, Nishio N, et al. Rapid, non-invasive fluorescence margin assessment: Optical specimen mapping in oral squamous cell carcinoma. Oral Oncol 2019;88:58–65.
[22] Reddy RS, Sai Praveen KN. Optical coherence tomography in oral cancer: A transpiring domain. J Cancer Res Ther 2017;13(6):883–8.
[23] Cho KJ, Song JS. Recent changes of classification for squamous intraepithelial lesions of the head and neck. Arch Pathol Lab Med 2018;142(7):829–32.